Preprints of the 21st IFAC World Congress (Virtual)
Berlin, Germany, July 12-17, 2020

Robust H_∞ Control for PWM Boost Converters Subject to Aging Capacitor Conditions ⋆

Caio dos S. Magalhães * **Bernardo Ordoñez** *
Humberto X. Araújo *

* *Electrical Engineering Department, Federal University of Bahia, Salvador, Brazil (e-mail: caio.santos@ufba.br, bordonez@ufba.br, humberto.araujo@ufba.br)*

Abstract: Electrolytic capacitors are extensively used in DC-DC power converters and consist of a major source of concern about system reliability. Although these components are heavily affected by aging, conventional modelling and control design for converters often disregard the uncertainty on capacitor parameters. In this paper, the robust control problem for boost converters is addressed with the derivation of a more comprehensive model. Although the modelling complexity is higher, the simplicity of linear state feedback control is preserved and the synthesis algorithm is performed by a LMI-based optimization problem. Moreover, the proposed control scheme requires state estimation, which is performed online as part of an identification system. Simulation results are presented and indicate the validity of the proposed concept.

Keywords: Application of power electronics, PWM boost converters, Robust optimal control, Modelling and simulation of power systems, Aging capacitors, Condition Monitoring

1. INTRODUCTION

Boost converters are power electronics devices designed to increase the voltage level between sources and loads, whilst maintaining the power loss minimal during the conversion process (Erikson and Maksimovic, 1999). Typical applications include aerospace industry (Mattos et al., 2018), powertrain interface (Hegazy et al., 2012) and photovoltaic systems (Dahmane et al., 2013). The most common control problem associated with those devices is the output voltage regulation, which must be kept within an operational range in spite of nonlinear dynamics and parameter uncertainties. Moreover, it is necessary to satisfy transient requirements and maximize disturbance rejection in order to assure the proper operation of the converter.

In several publications, robust control strategies for DC-DC converters were developed by proposing the design of nonlinear (Fadil and Giri, 2009; Al-Rabadi and Alsmadi, 2011) and linear (Ollala et al., 2010, 2011; Jr. et al., 2012) controllers. The last one consists of fixed state feedback gains that can be easily obtained through LMI-based methods, which have many advantages (Ollala et al., 2010, 2011). However, all those previous papers use converter models that disregard the influence of parasitic resistance on the inductor and capacitor, which might result in an underperforming controller or even system instability. The aforementioned papers also consider only the resistive load and switching duty cycle as uncertainities. As indicated in extensive literature (Aeloiza et al., 2005; Volgelsberger et al., 2011; Ren and Gong, 2018; Ren et al., 2019), boost converters widely employ aluminum electrolytic capacitors (AEC), which tend to undergo intense degradation during their lifespan owing to electrolyte evaporation. This aging leads to a progressive increase on the equivalent series resistance (ESR) and a decrease on capacitance. As a matter of fact, manufactures often consider that the AEC is at the end of their life cycle when its capacitance is reduced to 80% and/or the ESR reaches 2 or 3 times its initial value at the same temperature (Wang and Blaabjerg, 2014). An industrial survey (Yang et al., 2010) also suggests that capacitors are responsible for 30% of converter failures. Therefore, electrolytic capacitors are a major concern in converter reliability, which prompted many studies dedicated to online identification of the AEC parameters (notably ESR and capacitance) for health monitoring of power electronic circuits (see Aeloiza et al. (2005); Volgelsberger et al. (2011); Ren and Gong (2018)).

In order to combine offline robust linear LMI-based control with online parameter identification, this paper proposes a novel control design technique for the PWM boost converter. To address the aforementioned limitations, parasitic ESR effects are considered in the model for both inductor and capacitor, and a new polytopic region is derived to include the capacitor ESR and pure capacitance uncertainties. Furthermore, an online identification method is used to estimate the value of capacitor ESR and also as a state observer. Hence, the monitoring system is employed for both health checking and control purposes, which differs from previous works that only considered the control problem. The rest of the paper is organized as follows. Section 2 describes the linearized model of the boost converter and the novel polytope of uncertainties. Section 3 presents the robust H_∞ synthesis procedure and Section 4 exposes the monitoring system scheme. In Section 5,

⋆ The authors thank CAPES, "Coordenação de Aperfeiçoamento de Pessoal de Ensino Superior", for funding this work.

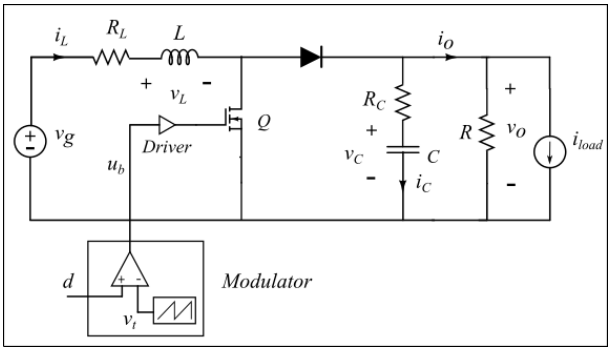

Fig. 1. Diagram of a PWM step-up converter.

simulation results are provided to validate the proposed concept. A brief conclusion is presented in Section 6.

2. BOOST CONVERTER MODELLED WITH UNCERTAINTIES

The PWM boost converter circuit is displayed in Fig. 1, where v_g is the input line voltage, v_o is the output voltage and i_{load} is the disturbance on the output current i_o. Both the inductor and the output capacitor are considered as a pure reactive component (L and C respectively) in series with a pure resistance (R_L and R_C respectively). The measurable signals are v_o and the currents across the inductor i_L and the capacitor i_C, whereas v_C is an unmeasurable state associated to the capacitor. The commutation process is controlled by the duty cycle signal d, which governs the transistor switching through a pulse-width modulator of frequency f_s and a drive circuit. For more information on PWM control applied to DC-DC converters, see Erikson and Maksimovic (1999).

2.1 Averaged model of a CCM boost converter

The converter is assumed to operate in continuous conduction mode (CCM). The theory of the averaged model is well-established in the literature (Erikson and Maksimovic, 1999; Bacha et al., 2014) and consists of disregarding the high frequency behavior due to the switching process. Only the low frequency components, which correspond to moving averages of the signals, are modelled for control purposes. For step-up converters, the averaged model is bilinear (Ollala et al., 2011), therefore it can be linearized and written as

$$\begin{cases} \dot{x}(t) = \mathbf{A}x(t) + \mathbf{B}_w w(t) + \mathbf{B}_u u(t) \\ z(t) = \mathbf{C}_z x(t) + \mathbf{D}_w w(t) + \mathbf{D}_u u(t), \end{cases} \tag{1}$$

where $\mathbf{A} \in \mathbb{R}^{n\times n}$, $\mathbf{B}_w \in \mathbb{R}^{n\times r}$, $\mathbf{B}_u \in \mathbb{R}^{n\times m}$, $\mathbf{C}_z \in \mathbb{R}^{p\times n}$, $\mathbf{D}_w \in \mathbb{R}^{p\times r}$, $\mathbf{D}_u \in \mathbb{R}^{p\times m}$ and

$$x(t) = \begin{bmatrix} i_L(t) \\ v_C(t) \\ x_{int}(t) \end{bmatrix}, \; w(t) = \begin{bmatrix} v_g(t) \\ i_{load}(t) \end{bmatrix}, \; u(t) = d(t)$$
$$\text{and } z(t) = v_o(t).$$

The artificial state $x_{int}(t)$ corresponds to the integral of the error between the voltage output $v_o(t)$ and the reference V_{ref}. In this arrangement, any stabilizing controller will provide output regulation on closed-loop steady state. Furthermore, it is considered in the model that the line voltage v_g is composed by a CC value V_g and a small AC disturbance $v_g(t)$, whose effects on the output must be mitigated along with those from $i_{load}(t)$. As previously mentioned, the state $v_c(t)$ cannot be directly measured, and its estimation will be part of the identification process. The state-space matrices are given by

$$\begin{aligned} \mathbf{A} &= \begin{bmatrix} -\dfrac{(R_L R + R_L R_C + D' R_C R)}{(R_C + R)L} & -\dfrac{D' R}{(R_C + R)L} & 0 \\ \dfrac{D' R}{(R_C + R)C} & -\dfrac{1}{(R_C + R)C} & 0 \\ \dfrac{D' R_C R}{R_C + R} & \dfrac{R}{R_C + R} & 0 \end{bmatrix}, \\ \mathbf{B}_w &= \begin{bmatrix} \dfrac{1}{L} & \dfrac{D' R_C R}{(R_C + R)L} \\ 0 & -\dfrac{R}{(R_C + R)C} \\ 0 & -\dfrac{R_C R}{R_C + R} \end{bmatrix}, \mathbf{B}_u = \begin{bmatrix} \dfrac{(R_C + D' R)V_C}{(R_C + R)D' L} \\ -\dfrac{V_C}{(R_C + R)D' C} \\ -\dfrac{R_C V_C}{(R_C + R)D'} \end{bmatrix}, \\ \mathbf{C}_z &= \begin{bmatrix} \dfrac{D' R_C R}{R_C + R} & \dfrac{R}{R_C + R} & 0 \end{bmatrix}, \mathbf{D}_w = \begin{bmatrix} 0 & -\dfrac{R_C R}{R_C + R} \end{bmatrix}, \\ \mathbf{D}_u &= \begin{bmatrix} -\dfrac{R_C V_C}{(R_C + R)D'} \end{bmatrix}, \end{aligned} \tag{2}$$

where D is the stationary average duty cycle, which is between 0 and 1, and $D' = 1 - D$ is its complementary value. The equilibrium points of the averaged states v_C and i_L are respectively given by

$$\begin{aligned} V_C &= \frac{D' R(R_C + R)V_g}{R_L R + R_L R_C + D' R_C R + D'^2 R^2}, \\ I_L &= \frac{V_C}{D' R} = \frac{(R_C + R)V_g}{R_L R + R_L R_C + D' R_C R + D'^2 R^2}. \end{aligned} \tag{3}$$

It must be pointed out that, since $v_o = v_C + R_C i_C = v_C + R_C C \dot{v_C}$, the averaged steady-state output V_o is equal to V_C. In effect, one can argue that it would be simpler to deduce a model using v_o as a state instead of v_c, as it would nullify the need for state estimation. However, as mentioned in Ren and Gong (2018), such method would lead to the derivative of the diode current, which is discontinuous between the commutation modes. Hence, as far as the authors know, it is not possible to derive an accurate continuous-time model for the step-up converter using the output voltage as a state.

2.2 Convex polytope of uncertainties

In this formulation, the parameters D', R, R_C and C are considered uncertain or slowly time-variant due to aging. All state-space matrices depend on those parameters, which are independent and in general can be grouped in an uncertainty vector $p = [p_1, \ldots, p_{n_p}]$. The limits of each parameter are known, i.e., $p_i \in [\underline{p_i}, \overline{p_i}]$. Thus the vector p belongs to the convex set $C_o(g_1, \ldots, g_L)$, where g_i represents the vertices of the convex polytope with $L = 2^{n_p}$. Moreover, if the matrices depend linearly on p, then there is another convex hull $C_o(\mathcal{G}_1, \ldots, \mathcal{G}_L)$ that contains all the possible combinations for the uncertain system, as expressed by the following

$$\begin{aligned} &[\mathbf{A}(p), \mathbf{B}_w(p), \ldots, \mathbf{D}_u(p)] \in C_o(\mathcal{G}_1, \ldots, \mathcal{G}_L) = \\ &\Big\{ \sum_{i=1}^{L} \sigma_i \mathcal{G}_i, \; \sigma_i \geq 0, \; \sum_{i=1}^{L} \sigma_i = 1 \Big\}. \end{aligned} \tag{4}$$

However, as it can be seen in (2), the relationship between the matrix entries and the uncertain parameters is not linear for the boost converter, which precludes the direct application of (4). In order to make this possible, the following parameters are defined

$$\begin{aligned}\beta &= \frac{1}{R_C+R},\ \mu = \frac{R}{R_C+R},\ \eta = \frac{D'R}{R_C+R},\\ \delta &= \frac{V_C R}{(R_C+R)D'V_g} = \frac{R^2}{R_L R + R_L R_C + D'R_C R + D'^2 R^2},\\ \epsilon &= \frac{(R_C+D'R)V_C}{(R_C+R)D'V_g} = \frac{D'R^2+R_C R}{R_L R + R_L R_C + D'R_C R + D'^2 R^2}.\end{aligned} \tag{5}$$

The state-space matrices can be rewritten as

$$\begin{aligned}\mathbf{A} &= \begin{bmatrix} -\frac{(R_L+R_C\eta)}{L} & -\frac{\eta}{L} & 0 \\ \frac{\eta}{C} & -\frac{\beta}{C} & 0 \\ R_C\eta & \mu & 0 \end{bmatrix},\\ \mathbf{B}_w &= \begin{bmatrix} \frac{1}{L} & \frac{R_C\eta}{L} \\ 0 & -\frac{\mu}{C} \\ 0 & -R_C\mu \end{bmatrix},\ \mathbf{B}_u = \begin{bmatrix} \frac{V_g\epsilon}{L} \\ -\frac{V_g\delta}{RC} \\ -\frac{R_C V_g \delta}{R} \end{bmatrix},\\ \mathbf{C}_z &= \begin{bmatrix} R_C\eta & \mu & 0 \end{bmatrix},\ \mathbf{D}_w = \begin{bmatrix} 0 & -R_C\mu \end{bmatrix},\\ \mathbf{D}_u &= \begin{bmatrix} -\frac{R_C V_g \delta}{R} \end{bmatrix}.\end{aligned} \tag{6}$$

In (6), there are still some nonlinearities involving uncertain parameters, such as R_C, R and C. However, the greatest contribution of this approach is to isolate η, ϵ and δ, parameters that depend mostly on D'. Since R_C and R_L tend to be much smaller than R, even considering aging and/or temperature effects, those three parameters might be approximated to $\eta \approx D'$, $\epsilon \approx \frac{1}{D'}$ and $\delta \approx \frac{1}{D'^2}$. Although these approximations will *not* be directly used, they suggest a less conservative polytopic covering. A similar approach is employed in Ollala et al. (2011), where an optimal convex hull is deduced to cover a 3D-line that represents the uncertainties of D'. However, since our problem do not disregard the effect of R_L and R_C, a new function of uncertainties is proposed

$$\begin{aligned}f(D', R_C, R) = \Big\{ &(\eta, \epsilon, \delta):\ D' \in \left[\underline{D'}, \overline{D'}\right],\\ &R_C \in \left[\underline{R_C}, \overline{R_C}\right],\ R \in \left[\underline{R}, \overline{R}\right] \Big\}.\end{aligned} \tag{7}$$

Since (7) represents a multivariable function, its graphical representation in $\mathbb{R}^3$ is a set of parameterized curves that form a solid. In Fig. 2, $f(D', R_C, R)$ is displayed considering $D' \in [0.3, 1.0]$, $R_C \in [0.2, 0.6]\Omega$, $R \in [20, 50]\Omega$ and $R_L = 0.4\Omega$. The simplest option for polytopic covering is expressed in Fig. 2, where the 8 vertices of the hyperrectangle are defined by the 8 possible combinations among the extreme values of each parameter η, ϵ and δ. Albeit technically correct, this strategy is far from optimal and can actually lead to an infeasible controller synthesis problem due to the excess of conservatism. A more functional method is proposed and consists of defining the vertices by optimal covering of plane projections. Since there are three variables of uncertainty and consequently

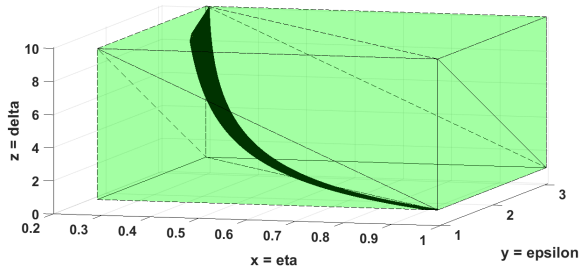

Fig. 2. Solid of uncertainties (in black).

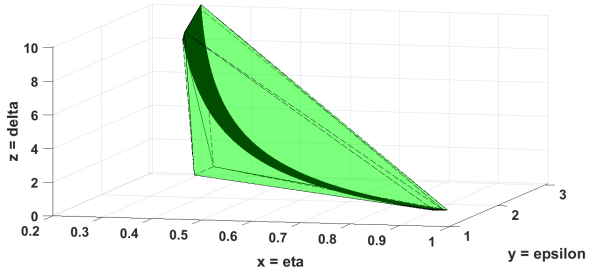

Fig. 3. Less conservative polytopic covering.

8 possible combinations of limit values, the first 8 vertices are locked and correspond to the ends of the solid. Only two more vertices are necessary to build a convex hull and they can be deduced by the optimal covering of each plane projection.

The 10 vertices of the convex hull are expressed in Table 1. Although the new polytope illustrated in Fig. 3 has more vertices than the old one in Fig. 2, its volume is much smaller (0.4356 against 13.4258), which translates into a huge reduction of modelling conservatism.

Table 1. Convex hull vertices.

x-axis(η)	Value	y-axis(ϵ)	Value	z-axis (δ)	Value
x_1	0.297	y_1	2.739	z_1	8.834
x_2	0.990	y_2	0.980	z_2	0.971
x_3	0.299	y_3	3.064	z_3	10.077
x_4	0.996	y_4	0.992	z_4	0.988
x_5	0.296	y_5	3.068	z_5	9.833
x_6	0.988	y_6	0.992	z_6	0.980
x_7	0.291	y_7	2.759	z_7	8.361
x_8	0.971	y_8	0.980	z_8	0.952
x_9	0.436	y_9	1.907	z_9	1.976
x_{10}	0.436	y_{10}	1.503	z_{10}	1.976

As aforementioned, even though $f(D', R_C, R)$ is a three-variable function, its dependence on D' is far stronger than the others. The idea of the convex hull is to isolate and treat separately the uncertainty on D'. Thus, η, ϵ and δ can be represented as a vertice v in the uncertain vector p, which leads to less conservatism. The other uncertain parameters can be individually included in the vector p as $[R_C, R, C, v]$, assuming $C \in \left[\underline{C}, \overline{C}\right]$. Hence, the final uncertain polytope has $L = 80$ vertices, considering all possible combinations among the vertices v and the extreme values of the other parameters. Therefore, the uncertainties in (4) can be expressed as follows

$$\begin{aligned}&\mathcal{G}_1 = [\mathbf{A}(p_1), \mathbf{B}_w(p_1), \ldots, \mathbf{D}_u(p_1)],\\ \text{where}\quad &p_1 = [\underline{R_C}, \underline{R}, \underline{C}, v_1], \ldots\\ &\mathcal{G}_{80} = [\mathbf{A}(p_{80}), \mathbf{B}_w(p_{80}), \ldots, \mathbf{D}_u(p_{80})],\\ \text{where}\quad &p_{80} = [\overline{R_C}, \overline{R}, \overline{C}, v_{10}].\end{aligned} \tag{8}$$

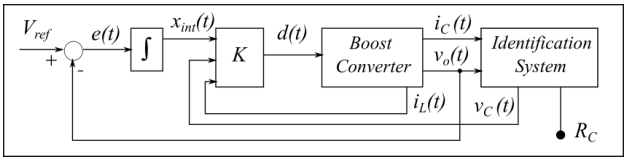

Fig. 4. Feedback control scheme

It is worthy to mention that the nonlinearities in the matrix entries do not invalidate the convex covering. This is due to the fact that the parameters are either strictly increasing (R_C and η) or strictly decreasing ($\frac{1}{R}$, $\frac{1}{C}$, ϵ and δ). Therefore, all the possible results for products and divisions are included in the final polytope formed by the combinations of the extremes.

3. ROBUST SYNTHESIS PROCEDURE

The proposed control system is displayed in Fig. 4. The main goal is to design a robust state-feedback controller to regulate the output voltage of the step-up DC-DC converter. The synthesis procedure is accomplished by a convex optimization problem with LMI constraints, described as follows.

3.1 LMI-based H_∞ constraint

Considering the system (1), the H_∞ norm of $H(s)$ is defined as (Zhou and Doyle, 1999)

$$\|H(s)\|_\infty = \sup_{w(t)\neq 0} \frac{\|z(t)\|_2}{\|w(t)\|_2}, \tag{9}$$

where $H(s)$ is the transfer matrix between the controlled output $z(t)$ and the disturbance (or exogenous input) $w(t)$. Based on Gahinet and Apkarian (1994), the uncertain system defined by (1) and (4) is stabilizable by a control law $u(t) = Kx(t)$ with $\|H(s)\|_\infty < \gamma$ if it exists a positive definite matrix $\mathbf{W} \in \mathbb{R}^{n\times n}$ and a matrix $\mathbf{Y} \in \mathbb{R}^{m\times n}$ such that the following LMIs hold

$$\begin{bmatrix} \mathbf{A}_i\mathbf{W} + \mathbf{W}\mathbf{A}_i' + \mathbf{B}_{u_i}\mathbf{Y} + \mathbf{Y}'\mathbf{B}_{u_i}' & \mathbf{B}_{w_i} & \mathbf{W}\mathbf{C}_{z_i}' + \mathbf{Y}'\mathbf{D}_{u_i}' \\ \mathbf{B}_{w_i}' & -\gamma\mathbf{I} & \mathbf{D}_{w_i}' \\ \mathbf{C}_{z_i}\mathbf{W} + \mathbf{D}_{u_i}\mathbf{Y} & \mathbf{D}_{w_i} & -\gamma\mathbf{I} \end{bmatrix} < 0,\ i = 1,\ldots,L, \tag{10}$$

and the controller gain is given by $K = \mathbf{Y}\mathbf{W}^{-1}$. Note that A_i, B_{u_i}, B_{w_i}, C_{z_i}, D_{u_i} and D_{w_i} are the vertices of polytope (4).

3.2 LMI-based pole placement constraints

Pole placement is directly associated with transient requirements, such as overshoot, settling time and rising time. Therefore, it is important to allocate the closed-loop poles to a desired region in the left half-plane. An example would be a $S(\alpha, \theta, \rho)$ region, which is defined by a vertical strip $a < -\alpha < 0$, a circle $|a \pm jb| < \rho$ and a conic sector $b < a\cot\theta$. Based on Chiliali and Gahinet (1996), it is possible to demonstrate that the uncertain system defined by (1) and (4) is stabilizable by a control law $u(t) = Kx(t)$ with all closed-loop poles inside the $S(\alpha, \theta, \rho)$ region if it exists a positive definite matrix $\mathbf{W} \in \mathbb{R}^{n\times n}$ and a matrix $\mathbf{Y} \in \mathbb{R}^{m\times n}$ such that the following LMIs hold

$$\mathbf{A}_i\mathbf{W} + \mathbf{W}\mathbf{A}_i' + \mathbf{B}_{u_i}\mathbf{Y} + \mathbf{Y}'\mathbf{B}_{u_i}' + 2\alpha\mathbf{W} < 0\ , \tag{11}$$

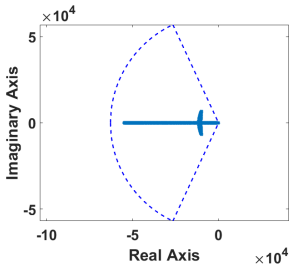

Fig. 5. Pole placement for possible uncertain plants.

$$\begin{bmatrix} -\rho\mathbf{W} & \mathbf{W}\mathbf{A}_i' + \mathbf{Y}'\mathbf{B}_{u_i}' \\ \mathbf{A}_i\mathbf{W} + \mathbf{B}_{u_i}\mathbf{Y} & -\rho\mathbf{W} \end{bmatrix} < 0\ , \tag{12}$$

$$\begin{bmatrix} \cos\theta(\mathbf{A}_i\mathbf{W} + \mathbf{W}\mathbf{A}_i' + \mathbf{B}_{u_i}\mathbf{Y} + \mathbf{Y}'\mathbf{B}_{u_i}') \\ \sin\theta(-\mathbf{A}_i\mathbf{W} + \mathbf{W}\mathbf{A}_i' - \mathbf{B}_{u_i}\mathbf{Y} + \mathbf{Y}'\mathbf{B}_{u_i}') \\ sin\theta(\mathbf{A}_i\mathbf{W} - \mathbf{W}\mathbf{A}_i' + \mathbf{B}_{u_i}\mathbf{Y} - \mathbf{Y}'\mathbf{B}_{u_i}') \\ \cos\theta(\mathbf{A}_i\mathbf{W} + \mathbf{W}\mathbf{A}_i' + \mathbf{B}_{u_i}\mathbf{Y} + \mathbf{Y}'\mathbf{B}_{u_i}') \end{bmatrix} < 0,\ i = 1,\ldots,L, \tag{13}$$

and the controller gain is given by $K = \mathbf{Y}\mathbf{W}^{-1}$.

3.3 Control Synthesis Algorithm

Finally, the state-feedback controller can be determined by a convex optimization problem written as

$$\min_{\mathbf{W}>0,\mathbf{Y}} \gamma \quad \text{subject to (10), (11), (12), and (13),} \tag{14}$$

where the controller gain is given by $K = \mathbf{Y}\mathbf{W}^{-1}$. Considering the parameters previously defined (Table 2), the algorithm is executed by standard MATLAB's LMI toolbox using $\alpha = 130$, $\rho = \frac{2\pi f_s}{10}$ and $\theta = 25°$. The designed controller is given by

$$K = [-0.3745 \quad -0.1730 \quad -71.5042] \tag{15}$$

with a guaranteed cost $\gamma = 12.847$ (22.18 dB). However, a robust analysis test based on Finsler's Lemma (Oliveira and Skelton, 2001) yields to $\gamma = 6.307$ (roughly 16 dB). This result is certainly more reliable, since this analysis method employs slack matrices, which makes it less conservative than the synthesis procedure. Figure 5 shows that, in spite of parameter deviations, the closed-loop poles are clustered inside $S(\alpha, \theta, \rho)$.

Table 2. Boost parameters.

Parameter	Value
R	$[20, 50]\Omega$
D'	$[0.3, 1.0]$
R_C	$[0.2, 0.6]\Omega$
C	$[96, 120]\mu F$
R_L	0.4Ω
L	$240\mu H$
V_g	$12V$
V_o, V_{ref}	$24V$
f_s	$100kHz$

4. IDENTIFICATION SYSTEM AND STATE ESTIMATION

As previously discussed, the state $v_C(t)$ is not physically measurable and therefore it requires estimation using the measurements of $v_o(t)$ and $i_c(t)$. This can be achieved by adapting the monitoring system used in Volgelsberger

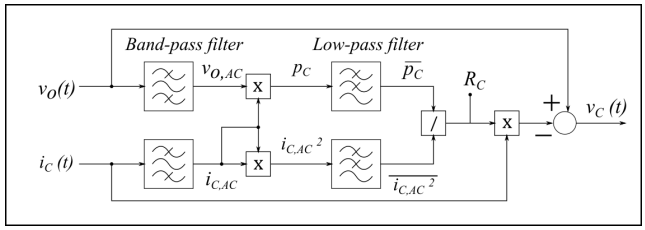

Fig. 6. Identification system adjusted to estimate $v_C(t)$.

et al. (2011) (see Figure 6), which was designed to identify the value of R_C online, and therefore assess the capacitor health. The principle applied is similar to that one in Aeloiza et al. (2005), where it is considered that the power loss on the capacitor p_C is exclusively owing to its ESR. Band-pass filters are used for extracting the AC components of the signals centered on the frequency at which the capacitor impedance is predominantly due to its ESR. Low-pass filters are utilized to obtain the DC components in order to compute the R_C value. It is important that both low-pass and band-pass filters are identical.

The proposed modification is to calculate $v_C(t)$ as $v_o(t) - R_C i_C(t)$. Since the identification of R_C is very fast and reliable, the estimation error is negligible. Moreover, the extra circuitry required is minimal since all the necessary variables for computation are already available. In this method, the identification process is integrated to the control system with low cost and preserving the benefits of both health monitoring and output voltage regulation.

5. SIMULATION RESULTS

In order to attest the validity of the proposed strategy, the closed-loop circuit of the boost converter is simulated in the software PSIM. The main objective will be to test disturbance dynamics caused by a load variation from 50Ω to 20Ω, which is the maximum power condition. Disturbance rejection is analyzed in both time and frequency domain under two different conditions: a new capacitor (defined by $R_C = 0.2\Omega$ and $C = 120\mu F$) and an aged capacitor ($R_C = 0.6\Omega$ and $C = 96\mu F$). R_C identification is also inspected to guarantee its effectiveness.

5.1 Load disturbance with new capacitor ($R_C = 0.2\Omega$)

Fig. 7 displays the output voltage subject to a step load variation that occurs halfway through the simulation. Note that the initial transient is well-behaved regardless of starting from the origin, and not the operational point at which the model was linearized. The second transient, which is caused by the load variation, also presents low overshoot, around 9.2%, and a settling time of approximately 6.4 ms (2% criteria).

As Fig. 8 depicts, the online R_C identification is very fast, accurate and barely affected by the load variation. The identified value rises only 1% after disturbance, which can be considered insignificant. Finally, the bode plots of $\frac{V_o(s)}{I_{load}(s)}$ (output impedance) are drawn using the AC sweep function of PSIM. The result is presented in Fig. 9. The magnitude peak is roughly 11.48 dB, which is in line with the guaranteed cost of 16 dB found in the Finsler analysis

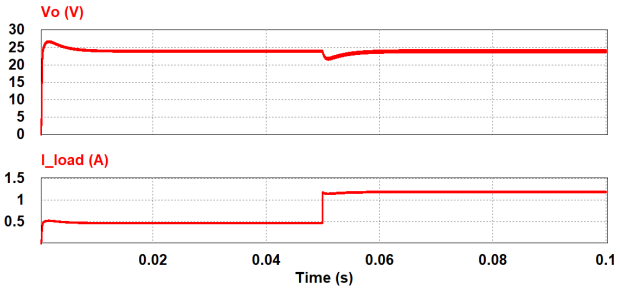

Fig. 7. Effect of load variation (50Ω to 20Ω) on the output voltage v_o with new capacitor.

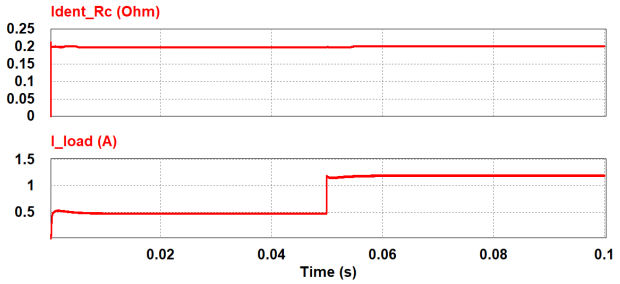

Fig. 8. Online R_C identification under load variation (50Ω to 20Ω) with new capacitor.

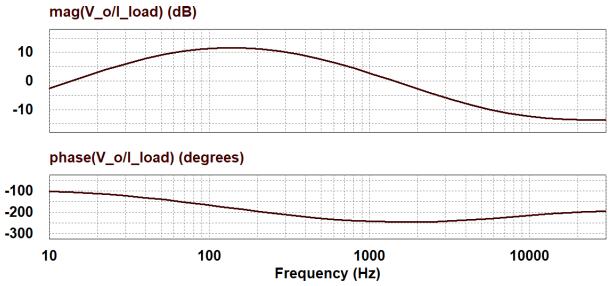

Fig. 9. Bode plots of $\frac{V_o(s)}{I_{load}(s)}$ with new capacitor.

step. Although the H_∞ norm reflects the influence of both disturbances (i_{load} and v_g) over the output v_o, i_{load} is the more impactful perturbation, which justifies a separate analysis for it.

5.2 Load disturbance with aged capacitor ($R_C = 0.6\Omega$)

The same tests were performed with an aged capacitor, whose ESR has increased 3 times and the capacitance decayed to 80% of its initial value. As Fig. 10 shows, the output dynamics under load change is similar to the previous case, except for a wider ripple on the output. However, this is expected since R_C is greater and the voltage ripple is approximately proportional to the capacitor ESR (Ren et al., 2019). Furthermore, the R_C identification is as efficient as the former case, displaying an estimation error even smaller (see Fig.11).

Finally, the bode plot of the output impedance is displayed in Fig. 12. The curves are very similar to those of the previous example, with a slight increase in the magnitude peak to 11.63 dB. Once again, the result is consistent with the Finsler analysis test, which suggests that the designed

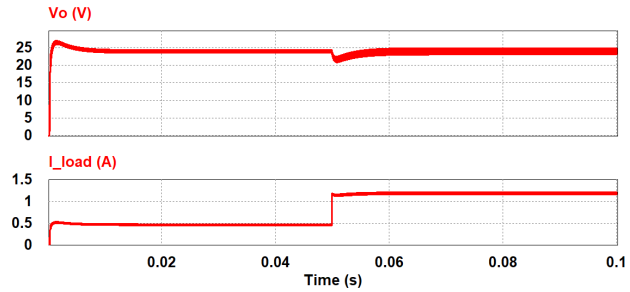

Fig. 10. Effect of load variation (50Ω to 20Ω) on v_o with aged capacitor.

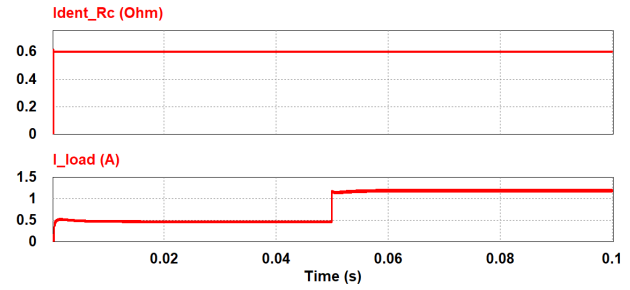

Fig. 11. Online R_C identification under load variation (50Ω to 20Ω) with aged capacitor.

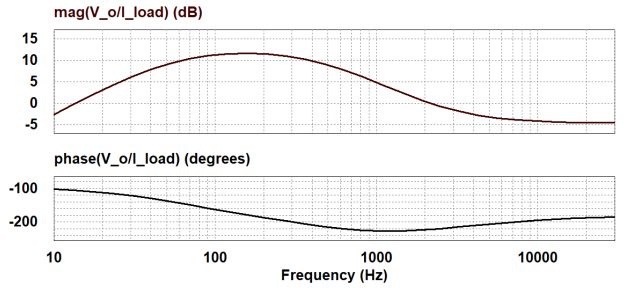

Fig. 12. Bode plots of $\frac{V_o(s)}{I_{load}(s)}$ with aged capacitor.

closed-loop converter abides by the specifications in spite of capacitor uncertainties.

6. CONCLUSION

This paper addresses robust H_∞ control for DC-DC power electronic converters and its main contribution is the emphasis on parameter uncertainties related to the output capacitor. It is proposed a more comprehensive uncertain model based on optimal polytopic covering, which avoids excess of conservatism. A novel control scheme is established by combining traditional state feedback with online parameter identification and state estimation for control purposes. The proposed strategy is validated by simulations. As a future work, a step-up converter circuit could be implemented in order to obtain experimental results.

ACKNOWLEDGEMENTS

Caio dos S. Magalhães is supported by a grant from CAPES, "Coordenação de Aperfeiçoamento de Pessoal de Ensino Superior", Brazil.

REFERENCES

Aeloiza, E., Kim, J., Ruminot, P., and Enjeti, P. (2005). A real time method to estimate electrolytic capacitor condition in PWM ajustable speed drives and uninterruptable power supplies. In *Proceedings of 36th Power Electronics Specialists Conference*, 2867–2872. IEEE.

Al-Rabadi, A. and Alsmadi, O. (2011). Supervised neural computing and LMI optimization for order model reduction-based control of the buck switching-mode power supply. *International Journal of Systems Science*, 42, 91–106.

Bacha, S., Munteanu, I., and Bractu, A. (2014). *Power Electronics Converters Models and Control*. Springer, London.

Chiliali, M. and Gahinet, P. (1996). H_∞ design with pole placement constraints: An LMI approach. *IEEE Transactions on Automatic Control*, 41, 358–367.

Dahmane, M., Bosche, J., and El-Hajjaji, A. (2013). Robust control approach for photovoltaic conversion system. In *Proceedings of 2013 International Renewable and Sustainable Energy Conference*, 123–129. IEEE.

Erikson, W. and Maksimovic, D. (1999). *Fundamentals of Power Electronics*. Klumer Academic Publishers, Massachusetts.

Fadil, H.E. and Giri, F. (2009). Robust nonlinear adaptive control of multiphase synchronous buck power converters. *Control Engineering Practice*, 17, 1245–1254.

Gahinet, P. and Apkarian, P. (1994). A linear matrix inequality approach H_∞ control. *International Journal of Robust and Nonlinear Control*, 4, 421–448.

Hegazy, O., Mierlo, J., and Lataire, P. (2012). Analysis, modeling and implementation of a multidevice interleved dc/dc converter for fuel cell hybrid electric vehicles. *IEEE Transactions Power Electronics*, 27, 4445–4458.

Jr., L.M., Montagner, V., Pinheiro, R., and Oliveira, R. (2012). Robust H_2 control applied to boost converters: design, experimental validation and performance analysis. *IET Control Theory and Applications*, 6, 1881–1888.

Mattos, E., Andrade, A., Hollweg, G., Pinheiro, J., and Martins, M. (2018). A review of boost converter analysis and design in aerospace applications. *IEEE Latin America Transactions*, 16, 305–313.

Oliveira, M. and Skelton, R. (2001). Stability tests for constrained linear systems. In S. Moheimani (ed.), *Perspectives in Robust Control*, volume 268, 241–257. Springer, London.

Ollala, C., Leyva, R., Aroudi, A.E., and Quiennec, I. (2010). LMI robust control design for boost PWM converters. *IET Power Electronics*, 3, 75–85.

Ollala, C., Leyva, R., Aroudi, A.E., and Quiennec, I. (2011). Robust optimal control of bilinear dc-dc converters. *Control Engineering Practice*, 19, 688–699.

Ren, L. and Gong, C. (2018). Modified hybrid model of boost converters for parameter identification of passive components. *IET Power Electronics*, 11, 764–771.

Ren, L., Gong, C., and Zhao, Y. (2019). An online esr estimation method for output capacitor of boost converter. *IEEE Transactions on Power Electronics*, 34, 10153–10165.

Volgelsberger, M., Wiesinger, T., and Ertl, H. (2011). Life-cycle monitoring and voltage-managing unit for dc-link electrolytic capacitors in PWM converters. *IEEE Transactions on Power Electronics*, 26, 493–503.

Wang, H. and Blaabjerg, F. (2014). Reliability of capacitors for dc-link applications in power electronics converters - an overview. *IEEE Transactions on Industrial Applications*, 50, 3569–3578.

Yang, S., Xiang, D., Bryant, A., Mawby, P., Ran, L., and Tavner, P. (2010). Condition monitoring for device reliability in power electronic converters: A review. *IEEE Transactions on Power Electronics*, 25, 2734–2752.

Zhou, K. and Doyle, J. (1999). *Essentials of robust control*. Prentice Hall, New Jersey.